CSIRO PUBLISHING

International Journal of Wildland Fire **2012**, *21*, 243–256
http://dx.doi.org/10.1071/WF10075

Assessment of post-fire changes in land surface temperature and surface albedo, and their relation with fire–burn severity using multitemporal MODIS imagery

Sander Veraverbeke[A,B,F], *Willem W. Verstraeten*[C,D], *Stefaan Lhermitte*[C,E], *Ruben Van De Kerchove*[A] *and Rudi Goossens*[A]

[A]Department of Geography, Ghent University, Krijgslaan 281 S8, BE-9000 Ghent, Belgium.
[B]Jet Propulsion Laboratory, California Institute of Technology, 4800 Oak Grove Drive, Pasadena, CA 91109, USA.
[C]Royal Netherlands Meteorological Institute, PO Box 201, NL-3730 AE, De Bilt, the Netherlands.
[D]Fluid Dynamics Department, Eindhoven University of Technology, Postbus 513, NL-5600, the Netherlands.
[E]Centro de Estudios Avanzados en Zonas Aridas, Universidad de la Serena, La Serena, Chile.
[F]Corresponding author. Email: sander.s.veraverbeke@jpl.nasa.gov

Abstract. This study evaluates the effects of the large 2007 Peloponnese (Greece) wildfires on changes in broadband surface albedo (α), daytime land surface temperature (LSTd) and night-time LST (LSTn) using a 2-year post-fire time series of Moderate Resolution Imaging Spectroradiometer satellite data. In addition, it assesses the potential of remotely sensed α and LST as indicators for fire–burn severity. Immediately after the fire event, mean α dropped up to 0.039 (standard deviation = 0.012) ($P < 0.001$), mean LSTd increased up to 8.4 (3.0) K ($P < 0.001$), and mean LSTn decreased up to −1.2 (1.5) K ($P < 0.001$) for high-severity plots ($P < 0.001$). After this initial alteration, fire-induced changes become clearly smaller and seasonality starts governing the α and LST time series. Compared with the fire-induced changes in α and LST, the post-fire NDVI drop was more persistent in time. This temporal constraint restricts the utility of remotely sensed α and LST as indicators for fire–burn severity. For the times when changes in α and LST were significant, the magnitude of changes was related to fire–burn severity, revealing the importance of vegetation as a regulator of land surface energy fluxes.

Additional keywords: climate, NDVI, remote sensing, satellite.

Received 14 July 2010, accepted 6 August 2011, published online 3 January 2012

Introduction

Biomass burning is a major disturbance in almost all terrestrial ecosystems (Dwyer *et al.* 2000; Pausas 2004; Riaño *et al.* 2007), partially or completely removing the vegetation layer and affecting post-fire vegetation composition (Epting and Verbyla 2005; Lentile *et al.* 2005). The fire-induced vegetation depletion causes abrupt changes in carbon, energy and water fluxes at local scale (Bremer and Ham 1999; Amiro *et al.* 2006*a*; Montes-Helu *et al.* 2009), thereby influencing species richness, habitats and community composition (Moretti *et al.* 2002; Capitanio and Carcaillet 2008). Understanding these local-scale changes in fluxes is therefore essential for management practices as they will have a strong effects on the water and energy balances (Bremer and Ham 1999; Amiro *et al.* 2006*a*), and may cause changes in circulation and regional heating patterns (Beringer *et al.* 2003; Wendt *et al.* 2007).

A key parameter in post-fire management is fire–burn severity. Fire–burn severity relates to the degree of environmental change caused by a fire (Key and Benson 2005). Although the terms fire and burn severity are often interchangeably used (Boer *et al.* 2008; Keeley 2009), some authors suggest clearly differentiating between them (Lentile *et al.* 2006; Veraverbeke *et al.* 2010*a*). By doing so, fire severity gauges the effect of fire in pre-recovery recovery phase, accounting solely for direct fire effects. Burn severity, in contrast, combines both the immediate effect of fire with ecosystems responses (mainly vegetation regeneration). The main driver for the terminological difference thus relies on the temporal dynamics of the post-fire environment (Key 2006; Veraverbeke *et al.* 2010*a*). Remote sensing has proved to be a time- and cost-effective means for mapping wildfire effects (among others Viedma *et al.* 1997; Stroppiana *et al.* 2002; Lentile *et al.* 2006; Riaño *et al.* 2007; van Leeuwen 2008). The remote sensing of burned area, fire–burn severity and vegetation regeneration mapping has a long tradition in the use of vegetation indices (VIs) (among others Cahoon *et al.* 1994; Barbosa *et al.* 1999;

Chafer *et al.* 2004; Chuvieco *et al.* 2008; French *et al.* 2008; Hernández Clemente *et al.* 2009). Although the ubiquitous Normalised Difference Vegetation Index (NDVI) relates reasonably well to fire–burn severity (Chafer *et al.* 2004; Hammill and Bradstock 2006; Veraverbeke *et al.* 2010*b*; Lhermitte *et al.* 2011), the Normalised Burn Ratio (NBR) has become increasingly popular as it consistently outperforms the NDVI for assessing immediate post-fire effects (Epting *et al.* 2005; French *et al.* 2008; Veraverbeke *et al.* 2010*b*). For monitoring post-fire vegetation recovery, however, the NDVI still is by far the most widely used index (among others Viedma *et al.* 1997; van Leeuwen 2008; Hernández Clemente *et al.* 2009; Lhermitte *et al.* 2010; van Leeuwen *et al.* 2010). Hitherto, few studies have assessed the potential of remotely sensed bioclimatic variables other than VIs with regards to post-fire effects. A suggestion on this topic originates from Lyons *et al.* (2008). In their study of the post-fire albedo changes in forested ecotypes in Alaska, they saw some potential in the use of a bi-temporally differenced metric based on surface albedo as a complementary index to the NBR for estimating fire–burn severity. To date, the majority of the post-fire effects studies have been conducted based on Landsat imagery because of its good spatial resolution for regional-scale studies (French *et al.* 2008). The use of Landsat imagery, however, can be constrained owing to cloud cover (Ju and Roy 2008) and image-to-image normalisation problems (Verbyla *et al.* 2008; Veraverbeke *et al.* 2010*c*). Owing to limited image availability, Landsat studies cannot fully account for the temporal dynamics of a post-fire environment. At the expense of spatial detail, low-resolution imagery with high temporal frequency presents a solution for this issue (Lhermitte *et al.* 2011; Veraverbeke *et al.* 2011).

Several field studies have assessed these effects of fire on bioclimatic variables. In this context, the surface blackening due to charring causes a clear albedo decrease immediately after the fire event (Bremer and Ham 1999; Beringer *et al.* 2003; Amiro *et al.* 2006*b*; Wendt *et al.* 2007; Tsuyuzaki *et al.* 2009). This decrease is up to half the prefire values (Bremer and Ham 1999) and the magnitude of change is dependent on the plot's fire severity (Beringer *et al.* 2003). This effect, however, is short-lived because albedo quickly recovers to prefire values when char materials are removed by weathering and vegetation starts to regenerate (Bremer and Ham 1999; Tsuyuzaki *et al.* 2009). After the initial short drop, albedo tends to increase during the next post-fire years, especially during the summer season, and the persistency of this increase is a function of the rate of vegetation regeneration (Amiro *et al.* 1999). Albedo values are subject to seasonality and as consequence dissimilarities between evergreen and deciduous ecotypes are evident. Summertime albedo is higher for deciduous ecosystems, whereas in winter differences are minor (Amiro *et al.* 2006*b*), although in winter snow cover often significantly affects the surface albedo (Betts and Ball 1997). Another typical post-fire change is an increase in Bowen ratio, which is defined as the ratio between sensible and latent heat fluxes (Bowen 1926; Beringer *et al.* 2003; Amiro *et al.* 2006*b*; Wendt *et al.* 2007). This is due to the decrease in latent heat flux and the consequent decrease in cooling by evapotranspiration (Wendt *et al.* 2007). The energy partitioning is, however, also subject to seasonal changes; the evaporative fraction, for example, will be higher during the wet season after the fire than immediately post-fire (Montes-Helu *et al.* 2009). It has also been demonstrated that evapotranspiration is considerably higher for regenerating deciduous forest stands compared with evergreens (Amiro *et al.* 2006*a*). Conversely, sensible and ground heat fluxes reveal a sharp increase shortly after the fire event. Consequently, soil and air temperatures are markedly higher after fire occurrence (Wendt *et al.* 2007). The measured temperature differences between burned and unburned control plots are generally up to 2–8 K (Amiro *et al.* 1999; Bremer and Ham 1999; Wendt *et al.* 2007; Montes-Helu *et al.* 2009). Persistency of these fire-induced microclimatic changes depends on fire severity (Beringer *et al.* 2003) and ecosystem type, ranging from ~1 year in grasslands (Bremer and Ham 1999) to up to several decades in forests (Amiro *et al.* 2006*b*). From a remote-sensing perspective, few studies have analysed spatiotemporal patterns of post-fire albedo and surface temperature. The studies that examined the effect of fire on surface heating all reported the expected temperature increase in the immediate post-fire environment (Lopez García and Caselles 1991; Cahoon *et al.* 1994; Eva and Lambin 1998; Lambin *et al.* 2003), whereas albedo values were halved immediately after the fire (Jin and Roy 2005; Lyons *et al.* 2008).

Traditional pre- and post-fire image differencing is impeded by temporal constraints (Key 2006; Verbyla *et al.* 2008; Veraverbeke *et al.* 2010*a*, 2010*b*, 2010*c*). Difficulties arise from both lag timing, i.e. time since fire, and seasonal timing. Even small interannual phenological differences can result in the detection of false trends (Key 2006; Verbyla *et al.* 2008; Lhermitte *et al.* 2011). To anticipate these false trends, Díaz-Delgado and Pons (2001) proposed comparing burned plots with unburned control plots within the same image. In this way, external and meteorological variations are minimised among the compared areas. Lhermitte *et al.* (2010) extended this rationale by making the control plot selection method spatially explicit. In contrast to the reference plot procedure of Díaz-Delgado and Pons (2001), the pixel-based method assigns a unique unburned control plot time series to each burned pixel, and as such, allowance is made for within-burn heterogeneity. This control plot selection is based on the similarity between the time series of the burned pixel and the time series of its surrounding unburned pixels for a prefire year (Lhermitte *et al.* 2010). So far, the pixel-based control plot selection procedure has only been used to analyse fire-induced changes in vegetation (Lhermitte *et al.* 2010; Veraverbeke *et al.* 2010*a*).

Hence, in this paper, post-fire changes in remotely sensed bioclimatic variables are monitored based on the control plot selection procedure. More specifically, we aim (i) to analyse post-fire changes in surface albedo and land surface temperature (LST), and (ii) to evaluate the potential of remotely sensed albedo and LST as indicators for fire–burn severity. The first objective aims to contribute to the understanding of how fire alters the environment, whereas the second goal meets the suggestion of Lyons *et al.* (2008) to test the potential of new metrics for assessing post-fire effects. The case study was conducted on the large 2007 Peloponnese (Greece) wildfires. The study makes use of multitemporal Moderate Resolution Imaging Spectroradiometer (MODIS) imagery.

Data and study area

Study area

The study focuses on several large fires that burned on the Peloponnese peninsula, in southern Greece (36°30′–38°30′N, 21–23°E) (Fig. 1). All the fires date from the 2007 summer. These fires were the worst natural disaster of the last decades in Greece, both in terms of human losses and the extent of the burned area. Elevation ranges between 0 and 2404 m above sea level. Limestone sediments cover most of the mountainous inland. Also, significant outcrops of sediments occur (Institute of Geology and Mineral Exploration 1983; Higgins and Higgins 1996). The hilly and mountainous inland is covered with shallow and gravelly soils (European Commission 2005). The climate is typically Mediterranean with hot, dry summers and mild, wet winters. At the Kalamata meteorological station (37°4′N, 22°1′E), the average annual temperature is 17.8°C and mean annual precipitation equals 780 mm (Fig. 2). The fires consumed more than 175 000 ha, which consisted of 57% shrub land, 21% coniferous forest, 20% olive groves and 2% deciduous forest (Veraverbeke *et al.* 2010*a*). A prefire land-cover map of the burned areas is given in Fig. 1. Black pine (*Pinus nigra*) is the dominant conifer species. The shrub layer is characterised by e.g. *Quercus coccifera*, *Q. frainetto*, *Pistacia lentiscus*, *Cistus salvifolius*, *C. incanus*, *Erica arborea*, *Sarcopoterum spinosum*. The olive groves consist of *Olea europaea* trees, whereas oaks are the dominant deciduous species. Mediterranean-type shrub lands are highly resilient to burning owing to both obligate seeder and resprouter fire-adapted strategies. They regenerate as a rule in a couple of years (Trabaud 1981; Capitanio and Carcaillet 2008) in a so-called autosuccession process (Hanes 1971). Conversely, the recovery of the forests is considerably slower and can take up to several decades (Viedma *et al.* 1997; van Leeuwen *et al.* 2010).

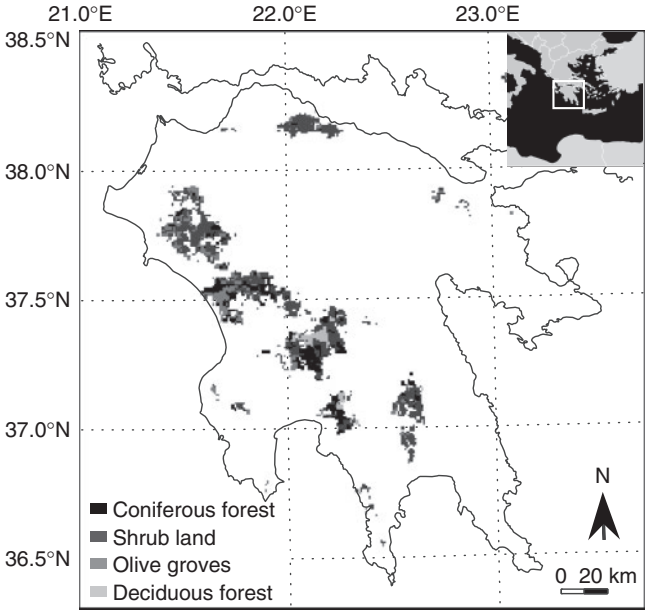

Fig. 1. Prefire land-cover map of the burned areas (after Veraverbeke *et al.* 2010*a*).

Data

MODIS satellite time series were used in this study. The MODIS sensor is on board the Terra and Aqua satellites and provides daily observations at 0130 hours (Aqua ascending node), 1030 hours (Terra descending node), 1330 hours (Aqua descending node) and 2230 hours (Terra ascending node) local time (Justice *et al.* 2002). Terra MODIS 16-day vegetation indices (1 km) (MOD13A2) (Huete *et al.* 2002), combined Terra and Aqua MODIS 16-day albedo (1 km) (MCD43B3) (Schaaf *et al.* 2002), Terra MODIS 8-day LST (1 km) (MOD11A2) and Aqua MODIS 8-day LST (1 km) (MYD11A2) with 1-K accuracy (Wan 2008) tiles covering the study area were acquired from the NASA Warehouse Inventory Search Tool (WIST) (https://wist.echo.nasa.gov, accessed 6 August 2011) for the period 1 January 2006 to 31 December 2009. NDVI, broadband (0.3–5.0 μm) white-sky albedo (α), daytime LST (LSTd), night-time LST (LSTn) and associated Quality Assurance (QA) layers were

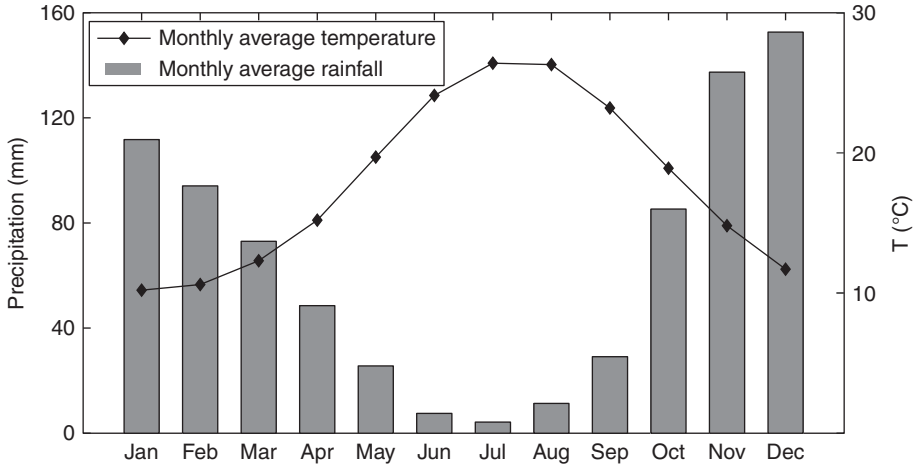

Fig. 2. Ombrothermic diagram of the Kalamata (Peloponnese, Greece) meteorological station (37°4′1″N 22°1′1″E) 1956–97 (Hellenic National Meteorological Service, www.hnms.gr, 6 August 2011).

subsequently extracted. We are aware that by using low-resolution imagery, spatial heterogeneity is sacrificed to some degree (Key 2006); however, recent research has highlighted the importance of the temporal dimension of post-fire effects (Veraverbeke *et al.* 2010*a*, 2011; Lhermitte *et al.* 2010). This explains our choice of low-resolution MODIS imagery, which is characterised by its high temporal frequency. The preprocessing steps included subsetting, reprojecting, compositing and creating continuous time series. The study area was clipped and the NDVI, α, LST and QA layers were reprojected into the Universal Transverse Mercator (UTM) with the World Geodetic System 84 (WGS 84) as geodetic datum. Subsequently, the 8-day LST layers were composited in 16-day composites using the Maximum Value Composite (MVC) criterion (Holben 1986). As such, the temporal resolution of the LST composites matches the NDVI and α composites temporal resolution. By applying the MVC criterion, high LST values are favoured. This is justified as previous research just indicated the importance of the post-fire temperature increase (Lopez García and Caselles 1991; Cahoon *et al.* 1994; Eva and Lambin 1998; Amiro *et al.* 1999; Bremer and Ham 1999; Lambin *et al.* 2003; Wendt *et al.* 2007; Montes-Helu *et al.* 2009). After compositing, a local second-order polynomial function, also known as an adaptive Savitzky–Golay filter (Savitzky and Golay 1964), was applied to the time series as implemented in the *TIMESAT* software (Jonsson and Eklundh 2004) to replace invalid observations. The *TIMESAT* program allows the inclusion of preprocessing. These masks are translated into weights, zero and one, that determine the uncertainty of the data values. Obscured observations were identified using the cloud, aerosol and snow algorithm flags of the QA layers. These flags consist of binary layers that permit a zero-weight value to be assigned to disturbed observations. Consequently these data do not influence the filter procedure. Owing to the low altitude (0–1000 m) of the burned areas, these locations do not experience permanent snow cover in the Mediterranean winter. In our study region, snow cover thus does not heavily affect ecosystem functioning. For this reason, we totally excluded snow effects from the analysis. Only the values of the masked observations were replaced to retain the original NDVI, α and LST values as much as possible.

Methodology

Control pixel selection

To minimise external and phenological variations, a pixel-based control plot selection method (Lhermitte *et al.* 2010) was implemented. This control pixel selection makes use of time series similarity and spatial context. The selection is based on the similarity of NDVI, α, and LST time series between burned pixels and their surrounding unburned pixels during the prefire year 2006, and the averaged Euclidian distance D was used as dissimilarity measure:

$$D = \frac{\sqrt{\sum_{t=1}^{n} (s\mathrm{NDVI}_t^f - s\mathrm{NDVI}_t^x)^2 + (s\alpha_t^f - s\alpha_t^x)^2 + (s\mathrm{LSTd}_t^f - s\mathrm{LSTd}_t^x)^2 + (s\mathrm{LSTn}_t^f - s\mathrm{LSTn}_t^x)^2}}{n} \quad (1)$$

where $s\mathrm{NDVI}_t^f$ is the burned focal pixel standardised NDVI time series, $s\mathrm{NDVI}_t^x$ is the unburned candidate control pixel standardised NDVI time series, $s\alpha_t^f$ is the focal pixel standardised α time series, $s\alpha_t^x$ is the candidate control pixel standardised α time series, $s\mathrm{LSTd}_t^f$ is the focal pixel standardised daytime LST time series, $s\mathrm{LSTd}_t^x$ is the candidate control pixel standardised daytime LST time series, $s\mathrm{LSTn}_t^f$ is the focal pixel standardised night-time LST time series, $s\mathrm{LSTn}_t^x$ is the candidate control pixel standardised night-time LST time series, and n is the number of observations in the prefire year ($n = 23$). The time series were standardised to provide equal weight to all data layers during the control pixel selection procedure. This standardisation was accomplished by the following formula:

$$sX = \frac{X - X_{mean}}{X_{sd}} \quad (2)$$

where sX is the standardised NDVI, α or LST, X is the original NDVI, α or LST, X_{mean} is the spatiotemporal mean NDVI, α or LST of all pixels, and X_{sd} represents the spatiotemporal NDVI, α or LST standard deviation of all pixels.

For valid control plot estimates, control pixels must correspond to the focal pixel if the fire had not occurred. First, this implies identical prefire characteristics for both control and focal pixels. Second, it means similar post-fire environmental conditions. To determine the appropriate control pixel selection criteria, the method of Lhermitte *et al.* (2010) was calibrated to our dataset based on post-fire similarity, because we wished to estimate how the NDVI, α and LST would have behaved in case of no fire occurrence. In this context, the accuracy of the control pixel selection is assessed by looking at the pre- and post-fire similarity of simulated burned pixels. This approach allows one to effectively assess how parameters c, the number of control pixels, and w × w, the window size around the focal pixel, affect the post-fire similarity. In this context, 500 unburned pixels were randomly selected and a simulated burning date was set for these pixels at the same composite date the real fire event took place. Subsequently, the sensitivity of dissimilarity criterion D to c and w × w was assessed for each of these pixels by comparing the outcome for varying numbers of control pixels (c = 1, 2,…, 15) and varying window sizes (3 × 3, 5 × 5,…, 25 × 25). The most similar control pixel was not the only one considered because a beneficial averaging that removes random noise in the time series has been noted in previous research (Lhermitte *et al.* 2010). As a result, the averaged time series of the two (or more) most similar pixels potentially provides better results. Evaluation consisted of measuring the temporal dissimilarity D for the 500 simulated burned sample pixels 1 year prefire and 1 year post-fire. This allows one to determine how well prefire similarity is maintained after a simulated burning date and how pre- and post-fire changes in similarity are related to the number of control pixels (c) and window size (w × w). More information on the control pixel selection procedure can be found in Lhermitte *et al.* (2010) and Veraverbeke *et al.* (2010*a*).

Analysis method

The control plot selection procedure allowed generation of 2-year post-fire time series of NDVI, α and LST (at 0130, 1030,

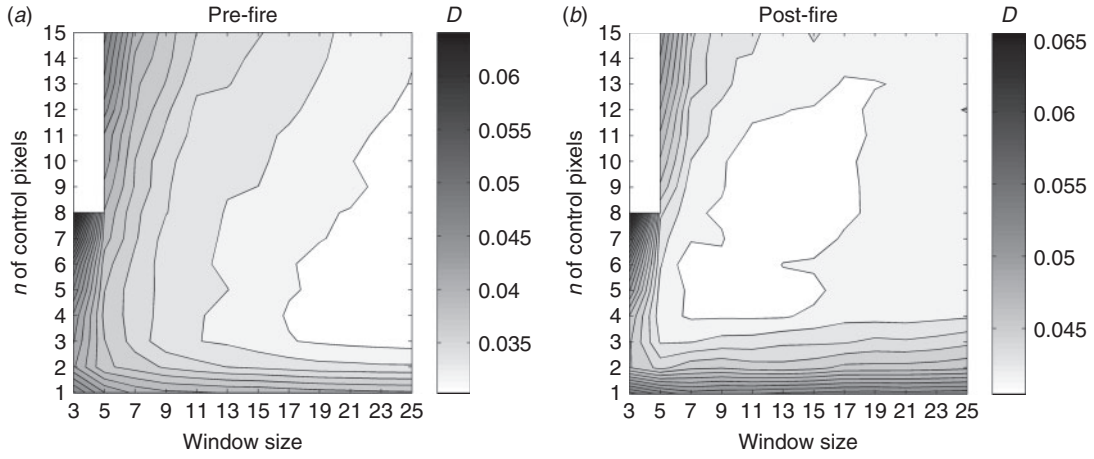

Fig. 3. Median dissimilarity *D* of the 500 sample pixels in function of varying number of control pixels and window size for (*a*) a prefire year, and for (*b*) a post-fire year. For the post-fire year, the same control pixels setting as in the prefire year is preserved. The grey scale reflects the temporal similarity, whereas the white areas in the upper-left corner represent impossible combinations (number of control pixels >8, for 3 × 3 window size).

1330 and 2230 hours local time) as best estimates of how these variables would have behaved without fire occurrence. We aimed to quantify the fire-induced changes in α and LST between focal and control pixels and to investigate their relationship with the changes in NDVI produced by fire. The mathematical formulation of these changes is:

$$dX_t = X_t^f - X_t^c \quad (3)$$

where X_t^f is the NDVI, α or LST value of the focal burned pixels at time t, X_t^c is the NDVI, α or LST of the control pixels and dX_t is the difference in NDVI, α or LST between focal and control pixels. The statistical significance of this difference is assessed by performing a z-test of the null hypothesis that dX_t follows a normal distribution with mean 0. Results are separately analysed for different land cover and fire–burn severity classes. Land-cover types were determined based on the classification of Veraverbeke *et al.* (2010*a*) resampled to a 1-km resolution (Fig. 1). As a proxy for fire–burn severity, we used a three-class equal interval differenced NDVI (dNDVI) stratification. For assessing immediate post-fire effects, the NBR generally results in a stronger correlation with field data than the NDVI (Epting *et al.* 2005; French *et al.* 2008); however, the NDVI's ability to capture the severity of fire-induced changes has been proved in a multitude of studies (among others Isaev *et al.* 2002; Díaz-Delgado *et al.* 2003; Chafer *et al.* 2004; Hammill and Bradstock 2006; Lhermitte *et al.* 2011). Specifically for the Peloponnese burns, Landsat dNDVI data related reasonably well with field data of severity ($R^2 = 0.46$, Veraverbeke *et al.* 2010*b*). To account for both immediate fire effects and vegetation recovery, which is prominent in a Mediterranean ecosystem over a 2-year post-fire period, we considered the NDVI appropriate. Although we recognise the spatial generalisation of low-resolution MODIS imagery compared with Landsat, previous research in the study area has demonstrated a relatively high correlation between Landsat spectral indices resampled to the MODIS resolution and MODIS spectral indices ($R^2 = 0.45$–0.59, Veraverbeke *et al.* 2010*a*, 2011). The choice of MODIS imagery is governed by its repeated temporal sampling, which is beneficial for considering the temporal dynamics of the post-fire environment (Veraverbeke *et al.* 2010*a*, 2011; Lhermitte *et al.* 2011). We considered a dynamic dNDVI stratification with three classes (LS, low severity; MS, moderate severity; HS, high severity) for the dates of composite images separately as reliable means of presenting and summarising results (White *et al.* 1996; Chafer *et al.* 2004; Hammill and Bradstock 2006; Escuin *et al.* 2008). By applying a separate stratification for each time step, we took into account the temporal component of post-fire effects (Key 2006; Lentile *et al.* 2006; Veraverbeke *et al.* 2010*a*). As we conducted a distinct analysis for each land-cover type, we did not use the relative version of a differenced spectral index as proposed by Miller and Thode (2007) to account for heterogeneity in prefire cover when assessing fire effects.

Results

Control pixel selection

Fig. 3*a* reflects *D* in function of varying numbers of control pixels and window size for a prefire year. It shows the median temporal similarity of the 500 unburned sample pixels. The median is used instead of the mean as it is more robust in the presence of outlier values. Two main effects are observed in the figure. First, the number of control pixels chosen influenced the dissimilarity measure owing to an averaging effect. The strength of this averaging effect was dependent on window size: the averaging effect became more important for larger window sizes. Second, there was a consistently decreasing trend in prefire *D* when window size increased. This feature appeared regardless of the number of control pixels chosen. This finding contrasts with what is visible in Fig. 3*b*, which represents the post-fire *D* in function of varying number of control pixels and window size. Here, one can see that *D* was at an optimum for intermediate window sizes. For the large window sizes, *D* started increasing again. As a result, differences between pre- and post-fire similarity increase for large windows. This effect originates from the possible selection of distant pixels that have

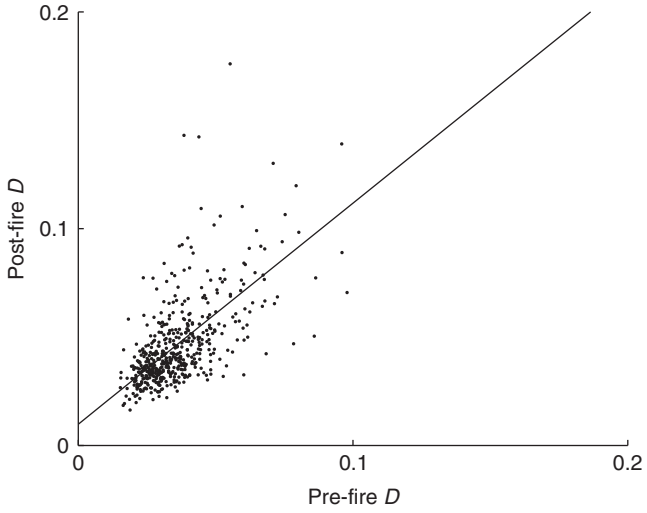

Fig. 4. Post-fire similarity *D* in function of prefire similarity *D* for the approach with the seven most similar pixels out of 120 candidate pixels.

a higher probability of showing different post-fire environmental conditions in larger windows (Lhermitte *et al.* 2010). As we wish to estimate the post-fire behaviour of NDVI, α and LST, post-fire similarity is the decision criterion to determine the control plot selection setting (Veraverbeke *et al.* 2010*a*). Based on Fig. 3*a–b*, the control pixel selection was calibrated by taking the average of the seven most similar pixels out of 120 candidate pixels ($11 \times 11 - 1$), which corroborates findings of Lhermitte *et al.* (2010) and Veraverbeke *et al.* (2010*a*).

Fig. 4 shows the relationship between the pre- and post-fire similarity *D* for the approach with the seven most similar pixels out of 120 candidate pixels. It reflects how prefire *D* provides an indicator for post-fire *D*. The majority of the pixels exhibit a linear relationship; however, two types of outliers occur. The first type of outliers represents data with relatively high prefire *D*. For these points, the selection results in a suboptimal control pixel. The second type of outliers has relatively elevated post-fire *D* values. These are pixels for which changes occurred after the simulated burning date. Fig. 4 shows that the outliers only represent a small fraction of the data cloud. As such, prefire *D* can be considered as a good indicator for post-fire *D* for the majority of the pixels.

Post-fire NDVI changes

The following sections summarise results of the post-fire changes in NDVI, α and LST. To avoid listing numbers in the text, Tables 1 and 2 tabulate some absolute values of changes for exemplary dates. In this respect, Tables 1–2 are complementary to Figs 5–8.

Fig. 5*a–d* shows the post-fire development of focal and control pixels mean NDVI per land-cover type. One can clearly infer the immediate post-fire drop. This drop was more explicit for forests than for shrub land and olive groves. After this initial decrease, the effects of both vegetation regeneration and seasonality became apparent. Fig. 5*e–h* displays the post-fire dNDVI values per land-cover type. For all land-cover types, the magnitude of the dNDVI change decreases when time passes; however, interannual differences remain visible. The crosses in the figure indicate when the mean value significantly deviates from zero ($P < 0.001$). Except from some observations in the deciduous forest class, all post-fire NDVI changes are statistically significant.

Post-fire α changes

In Fig. 6*a–d*, the post-fire trends in α for control and focal pixels are plotted per land-cover type. One can see an immediate post-fire α drop for all covers. During the 1-year post-fire summer, the focal pixels α of evergreen covers (shrub land, olive groves and coniferous forest) exceeded the control pixels values. This α increase was even more evident during the second post-fire summer. During winter periods, α changes were small. In Fig. 6*e–h*, one can see the temporal development and significance of differenced α (dα) values per land-cover type. In contrast with the majority of the summer observations, winter changes in α are not significant for most of the observations. Post-fire α changes per severity class are presented in Fig. 6*i–l*. The magnitude of the post-fire drop was related to fire severity and land-cover class. For forested covers, the α decrease was larger. For deciduous forest, for example, the α drop was up to 0.039 (0.012) for the HS class ($P < 0.001$). For the evergreen land-cover types, the α change of the HS class had already become positive during the first post-fire winter. In two summers post-fire this resulted in an increased α of, e.g. 0.016 (0.009) for coniferous forest ($P < 0.001$). The α changes in LS and MS classes were minor. Except for the immediate post-fire drop, differences in α changes between the severity classes are less obvious for deciduous forest.

Post-fire LSTd changes

Results of the MODIS Terra and Aqua LST analyses revealed very similar trends. As a consequence, only the Aqua LST analysis is presented. Fig. 7*a–d* depicts the mean LSTd of the control and focal pixels per land-cover class. In all land covers, the fire caused a clear LSTd increase immediately post-fire and during the subsequent summer periods, whereas in winter, changes were minor. The magnitude of the LSTd increase during subsequent summers became smaller as time elapsed. In Fig. 7*e–h*, the mean differenced LSTd (dLSTd) is plotted for the 2-year post-fire period. Regardless of land-cover type, one can see that the post-fire LSTd changes are significant during summer periods, whereas during winter periods, many observations did not reveal a significant difference. Fig. 7*i–l* presents the dLSTd changes per severity class. It is clear that the magnitude of the dLSTd change depends on land cover and severity class. For the HS class of coniferous forest, for example, the immediate post-fire dLSTd increase equalled 8.4 (3.0) K, whereas during the first and second post-fire summers, dLSTd values of 5.4 (2.3) K and 1.7 (1.2) K were obtained ($P < 0.001$). During winter, changes were minor and even sporadically negative, although these observations were not significant.

Post-fire LSTn changes

Fig. 8*a–d* depicts the 2-year post-fire temporal evolution of mean LSTn of the control and focal pixels per land-cover class. In these plots, it is very difficult to discriminate between the

Table 1. Post-fire mean (s.d.) Normalised Difference Vegetation Index (NDVI), surface albedo α daytime land surface temperature (LSTd) and night-time land surface temperature (LSTn) changes of control and focal pixels per land cover type for some exemplary moments

Some exemplary moments are: 29-Aug-07, first post-fire observation; 19-Dec-07, post-fire winter; 27-Jun-08, 1-year post-fire summer; 20-Dec-08, 1-year post-fire winter; 26-Jun-09, 2-year post-fire summer; and 19-Dec-09, 2-year post-fire winter

	29-Aug-07	19-Dec-07	27-Jun-08	20-Dec-08	26-Jun-09	19-Dec-09
Shrub land						
Mean NDVI control (s.d.)	0.46 (0.06)	0.60 (0.05)	0.50 (0.06)	0.62 (0.06)	0.52 (0.06)	0.69 (0.05)
Mean NDVI focal (s.d.)	0.30 (0.06)	0.47 (0.10)	0.38 (0.06)	0.53 (0.07)	0.44 (0.07)	0.65 (0.07)
Mean α control (s.d.)	0.140 (0.012)	0.120 (0.011)	0.149 (0.012)	0.122 (0.012)	0.142 (0.011)	0.127 (0.015)
Mean α focal (s.d.)	0.117 (0.018)	0.114 (0.020)	0.154 (0.014)	0.124 (0.021)	0.151 (0.014)	0.135 (0.020)
Mean LSTd control (s.d.) (K)	312.1 (2.1)	285.3 (1.7)	313.1 (2.5)	283.6 (2.0)	310.0 (2.5)	290.4 (1.5)
Mean LSTd focal (s.d.) (K)	316.6 (2.9)	285.7 (1.9)	315.2 (2.6)	283.7 (1.7)	311.2 (2.6)	290.0 (2.1)
Mean LSTn control (s.d.) (K)	291.4 (1.6)	275.0 (1.7)	292.6 (1.6)	274.0 (1.3)	290.5 (1.8)	282.0 (1.5)
Mean LSTn focal (s.d.) (K)	291.3 (1.9)	274.8 (1.8)	292.7 (1.7)	273.9 (1.5)	290.5 (1.9)	281.5 (2.0)
Olive groves						
Mean NDVI control (s.d.)	0.48 (0.04)	0.67 (0.04)	0.50 (0.05)	0.71 (0.03)	0.54 (0.04)	0.75 (0.03)
Mean NDVI focal (s.d.)	0.32 (0.05)	0.53 (0.09)	0.40 (0.05)	0.61 (0.06)	0.47 (0.05)	0.71 (0.06)
Mean α control (s.d.)	0.137 (0.014)	0.114 (0.011)	0.146 (0.010)	0.119 (0.010)	0.138 (0.008)	0.126 (0.012)
Mean α focal (s.d.)	0.115 (0.017)	0.109 (0.019)	0.149 (0.012)	0.123 (0.019)	0.146 (0.010)	0.137 (0.020)
Mean LSTd control (s.d.) (K)	311.5 (1.6)	286.2 (1.2)	313.1 (1.9)	284.3 (1.5)	309.2 (2.2)	291.4 (2.3)
Mean LSTd focal (s.d.) (K)	315.9 (2.6)	286.7 (1.3)	315.0 (2.0)	284.6 (1.6)	310.3 (2.3)	291.5 (1.9)
Mean LSTn control (s.d.) (K)	292.6 (1.0)	277.1 (1.5)	293.9 (0.9)	275.5 (1.2)	291.3 (1.2)	283.2 (1.2)
Mean LSTn focal (s.d.) (K)	292.6 (1.1)	276.8 (1.6)	294.1 (1.0)	275.4 (1.4)	291.3 (1.3)	282.9 (1.9)
Coniferous forest						
Mean NDVI control (s.d.)	0.60 (0.06)	0.67 (0.04)	0.63 (0.06)	0.71 (0.03)	0.63 (0.05)	0.77 (0.05)
Mean NDVI focal (s.d.)	0.36 (0.09)	0.41 (0.10)	0.41 (0.08)	0.55 (0.08)	0.51 (0.07)	0.69 (0.08)
Mean α control (s.d.)	0.124 (0.011)	0.100 (0.012)	0.134 (0.009)	0.102 (0.012)	0.127 (0.008)	0.102 (0.014)
Mean α focal (s.d.)	0.093 (0.014)	0.088 (0.020)	0.135 (0.013)	0.102 (0.021)	0.134 (0.011)	0.108 (0.021)
Mean LSTd control (s.d.) (K)	309.5 (1.9)	283.9 (1.6)	310.1 (2.2)	281.9 (1.6)	307.0 (1.5)	289.9 (1.8)
Mean LSTd focal (s.d.) (K)	314.8 (3.9)	284.4 (2.1)	313.4 (2.8)	283.2 (2.0)	308.8 (2.1)	289.6 (2.2)
Mean LSTn control (s.d.) (K)	291.7 (1.1)	275.4 (1.7)	292.9 (1.2)	274.5 (1.2)	290.5 (1.0)	282.4 (1.5)
Mean LSTn focal (s.d.) (K)	291.2 (1.6)	274.9 (1.8)	292.7 (1.6)	274.0 (1.0)	290.2 (1.2)	281.9 (2.0)
Deciduous forest						
Mean NDVI control (s.d.)	0.56 (0.06)	0.55 (0.04)	0.65 (0.07)	0.53 (0.06)	0.65 (0.06)	0.64 (0.06)
Mean NDVI focal (s.d.)	0.37 (0.08)	0.44 (0.07)	0.48 (0.08)	0.49 (0.05)	0.56 (0.08)	0.64 (0.06)
Mean α control (s.d.)	0.137 (0.009)	0.112 (0.008)	0.142 (0.007)	0.112 (0.010)	0.135 (0.005)	0.110 (0.007)
Mean α focal (s.d.)	0.109 (0.016)	0.091 (0.012)	0.140 (0.009)	0.104 (0.019)	0.133 (0.007)	0.111 (0.010)
Mean LSTd control (s.d.) (K)	310.1 (2.4)	283.8 (1.3)	310.6 (2.4)	283.0 (1.9)	307.3 (1.9)	289.7 (1.6)
Mean LSTd focal (s.d.) (K)	316.0 (3.7)	284.1 (1.4)	313.4 (2.7)	283.3 (2.3)	308.5 (2.0)	289.1 (1.9)
Mean LSTn control (s.d.) (K)	289.6 (1.0)	273.4 (0.5)	290.8 (0.8)	272.9 (0.6)	288.9 (0.8)	280.8 (0.6)
Mean LSTn focal (s.d.) (K)	289.0 (1.0)	274.0 (0.6)	290.8 (0.9)	272.7 (0.7)	288.5 (0.9)	280.2 (1.3)

control and focal pixels. Thus, changes in LSTn were very small. This is also illustrated in Fig. 8*e–h*, which show the mean dLSTn values per land-cover type. Results show a tendency of post-fire LSTn decrease. Except for the persistent significance of the post-fire LSTn decrease over coniferous forest, most changes were insignificant. Fig. 8*i–l* presents the mean dLSTn per severity class. The relationship between severity class and dLSTn was also only clear for coniferous forest. For the HS class of coniferous forest, for example, a consistent LSTn decrease was observed up to values of −1.4 (1.0) K during the 1-year post-fire winter.

Discussion

Control pixel selection

The strength of the control pixel selection procedure is its ability to mimic a burned pixel's behaviour as if there had not been a fire. The method therefore assesses the similarity in the temporal profiles of a burned pixel and its closest unburned neighbour pixels. By doing so, the procedure implicitly tends to select control pixels that exhibit similar vegetation (e.g. type, density) and environmental (e.g. topography, geology, climatology) conditions. The actual selection relies on prefire similarity, as post-fire similarity information is unavailable after the burning date. However, only considering prefire time series would not account for interannual meteorological variations. For this reason, a calibration was set up based on 500 simulated burned pixels. This calibration allows assessment of the relationship between pre- and post-fire similarity. As inferred from Fig. 3*b*, in contrast with Fig. 3*a*, the most optimal setting tends to select control pixels relatively close to the burned pixels. This effect arises from the selection of distant pixels with different post-fire meteorological conditions for larger window sizes (Lhermitte *et al.* 2010; Veraverbeke *et al.* 2010*a*). Fig. 4 demonstrates that

Table 2. Post-fire mean (s.d.) differenced albedo (dα), daytime land surface temperature (LSTd) and night-time land surface temperature (LSTn) values per land cover type and fire–burn severity class for some exemplary moments

Burn severity classes are: LS, low severity; MS, moderate severity; and HS, high severity. Some exemplary moments are: 29-Aug-07, first post-fire observation; 19-Dec-07, post-fire winter; 27-Jun-08, 1-year post-fire summer; 20-Dec-08, 1-year post-fire winter; 26-Jun-09, 2-year post-fire summer; and 19-Dec-09, 2-year post-fire winter. Values that significantly differ from zero ($P < 0.001$) are italicised

	29-Aug-07	19-Dec-07	27-Jun-08	20-Dec-08	26-Jun-09	19-Dec-09
Shrub land						
Mean dα LS (s.d.)	*−0.013* (*0.012*)	*−0.009* (*0.013*)	0.000 (0.007)	0.000 (0.014)	*0.005* (*0.008*)	*0.006* (*0.016*)
Mean dα MS (s.d.)	*−0.024* (*0.014*)	*−0.006* (*0.016*)	*0.005* (*0.010*)	0.002 (0.018)	*0.009* (*0.010*)	*0.008* (*0.017*)
Mean dα HS (s.d.)	*−0.032* (*0.011*)	0.000 (0.020)	*0.012* (*0.011*)	0.016 (0.025)	*0.012* (*0.012*)	0.013 (0.023)
Mean dLSTd LS (s.d.) (K)	*1.8* (*1.7*)	*0.2* (*0.8*)	*0.5* (*1.2*)	0.0 (1.1)	*0.7* (*1.1*)	−0.3 (2.0)
Mean dLSTd MS (s.d.) (K)	*4.5* (*2.5*)	*0.4* (*1.1*)	*2.1* (*1.9*)	0.1 (1.2)	*1.2* (*1.3*)	−0.3 (2.0)
Mean dLSTd HS (s.d.) (K)	*6.6* (*2.3*)	*0.8* (*1.5*)	*4.3* (*1.9*)	−0.4 (1.1)	*1.9* (*1.9*)	−0.8 (2.5)
Mean dLSTn LS (s.d.) (K)	0.0 (0.8)	−0.1 (0.8)	0.2 (0.8)	*−0.1* (*0.7*)	0.1 (0.7)	*−0.3* (*1.6*)
Mean dLSTn MS (s.d.) (K)	−0.1 (1.1)	*−0.2* (*0.8*)	*0.1* (*0.8*)	*−0.2* (*0.9*)	0.0 (0.8)	*−0.5* (*1.6*)
Mean dLSTn HS (s.d.) (K)	*−0.4* (*1.2*)	−0.3 (0.9)	−0.1 (0.9)	−0.3 (1.5)	−0.3 (1.4)	−1.4 (2.3)
Olive groves						
Mean dα LS	*−0.015* (*0.011*)	*−0.007* (*0.014*)	*0.002* (*0.007*)	0.001 (0.015)	*0.007* (*0.007*)	*0.011* (*0.017*)
Mean dα MS	*−0.022* (*0.012*)	*−0.005* (*0.015*)	*0.003* (*0.009*)	*0.004* (*0.016*)	*0.009* (*0.008*)	*0.011* (*0.018*)
Mean dα HS	*−0.029* (*0.011*)	0.000 (0.015)	0.007 (0.012)	*0.030* (*0.019*)	*0.019* (*0.014*)	0.014 (0.028)
Mean dLSTd LS (s.d.) (K)	*2.8* (*1.6*)	*0.3* (*0.9*)	*1.0* (*1.0*)	0.2 (0.9)	*0.8* (*0.9*)	−0.1 (1.7)
Mean dLSTd MS (s.d.) (K)	*4.4* (*2.1*)	*0.5* (*1.0*)	*1.8* (*1.5*)	*0.3* (*1.0*)	*1.2* (*1.1*)	0.0 (1.8)
Mean dLSTd HS (s.d.) (K)	*6.5* (*1.4*)	0.6 (1.3)	*3.5* (*2.1*)	−0.9 (1.0)	*2.1* (*1.7*)	0.0 (1.1)
Mean dLSTn LS (s.d.) (K)	0.0 (0.5)	−0.1 (0.7)	0.0 (0.5)	−0.1 (0.7)	0.0 (0.5)	−0.1 (1.4)
Mean dLSTn MS (s.d.) (K)	0.0 (0.6)	*−0.3* (*0.6*)	*0.2* (*0.6*)	−0.1 (0.8)	0.0 (0.7)	*−0.3* (*1.4*)
Mean dLSTn HS (s.d.) (K)	−0.1 (0.6)	*−0.6* (*0.7*)	0.2 (0.7)	−0.2 (1.1)	0.0 (0.7)	−0.7 (0.9)
Coniferous forest						
Mean dα LS	*−0.026* (*0.014*)	*−0.014* (*0.018*)	−0.005 (0.011)	−0.004 (0.019)	*0.004* (*0.009*)	*0.007* (*0.019*)
Mean dα MS	*−0.030* (*0.012*)	*−0.011* (*0.018*)	0.002 (0.012)	0.000 (0.020)	*0.007* (*0.010*)	*0.006* (*0.019*)
Mean dα HS	*−0.036* (*0.009*)	−0.004 (0.018)	*0.006* (*0.012*)	0.003 (0.026)	*0.016* (*0.009*)	*0.006* (*0.019*)
Mean dLSTd LS (s.d.) (K)	*2.9* (*2.3*)	0.3 (1.3)	*1.5* (*1.7*)	0.3 (1.4)	*1.1* (*1.3*)	−0.2 (2.1)
Mean dLSTd MS (s.d.) (K)	*5.3* (*3.2*)	*0.5* (*1.5*)	*3.3* (*2.2*)	0.2 (1.4)	*1.7* (*1.5*)	*−0.4* (*2.1*)
Mean dLSTd HS (s.d.) (K)	*8.4* (*3.0*)	0.6 (1.8)	*5.4* (*2.3*)	−0.4 (1.6)	*1.7* (*1.2*)	−0.3 (2.3)
Mean dLSTn LS (s.d.) (K)	−0.2 (0.8)	−0.2 (0.7)	0.1 (0.6)	−0.1 (0.7)	−0.1 (0.5)	−0.3 (1.4)
Mean dLSTn MS (s.d.) (K)	*−0.6* (*1.1*)	*−0.5* (*0.9*)	*−0.2* (*0.9*)	*−0.5* (*0.9*)	*−0.3* (*0.7*)	*−0.4* (*1.5*)
Mean dLSTn HS (s.d.) (K)	*−1.2* (*1.5*)	*−1.0* (*1.0*)	*−0.9* (*1.1*)	*−1.4* (*1.0*)	*−0.8* (*0.8*)	−0.8 (1.6)
Deciduous forest						
Mean dα LS	*−0.016* (*0.011*)	*−0.018* (*0.013*)	0.000 (0.009)	−0.013 (0.010)	0.006 (0.006)	0.000 (0.008)
Mean dα MS	*−0.030* (*0.012*)	*−0.021* (*0.015*)	−0.002 (0.008)	−0.008 (0.022)	−0.002 (0.008)	0.000 (0.009)
Mean dα HS	*−0.039* (*0.012*)	*−0.026* (*0.024*)	−0.006 (0.007)	0.002 (0.034)	−0.004 (0.007)	0.002 (0.012)
Mean dLSTd LS (s.d.) (K)	*2.8* (*2.4*)	*0.4* (*0.6*)	0.3 (1.4)	0.7 (0.8)	0.4 (0.6)	−0.6 (2.2)
Mean dLSTd MS (s.d.) (K)	*5.3* (*3.2*)	*0.4* (*0.8*)	*2.8* (*2.1*)	0.3 (1.2)	*0.8* (*1.2*)	−0.7 (2.0)
Mean dLSTd HS (s.d.) (K)	*8.1* (*2.0*)	0.0 (1.2)	*5.0* (*1.2*)	0.2 (1.1)	*2.1* (*1.6*)	0.2 (2.0)
Mean dLSTn LS (s.d.) (K)	−0.2 (0.5)	*0.8* (*0.6*)	0.5 (0.4)	−0.3 (0.6)	0.0 (0.5)	−0.6 (1.7)
Mean dLSTn MS (s.d.) (K)	*−0.6* (*0.8*)	*0.5* (*0.7*)	−0.1 (0.8)	−0.2 (0.6)	*−0.2* (*0.5*)	*−0.6* (*1.4*)
Mean dLSTn HS (s.d.) (K)	*−1.0* (*0.9*)	−0.2 (0.5)	−0.5 (0.9)	0.0 (0.4)	*−0.8* (*0.7*)	−0.3 (1.0)

prefire similarity is a valid indicator of post-fire similarity for the majority of the pixels. For some pixels, however, the selected control pixel will be suboptimal. This is especially true for control pixels that experienced considerable changes, such as land-management practices, after the fire date. A comprehensive discussion on the control pixel selection procedure can be found in Lhermitte *et al.* (2010) and Veraverbeke *et al.* (2010*a*).

Post-fire NDVI changes

Fig. 5 confirms the utility of the NDVI for monitoring fire-induced changes. The NDVI time series, however, are also subject to seasonal variations. The timing of image acquisition, both in terms of lag and seasonal timing, thus affects the NDVI response (Key 2006; Verbyla *et al.* 2008; Veraverbeke *et al.* 2010*a*; Lhermitte *et al.* 2011). The seasonality of the NDVI response also depends on land-cover type. In our study, deciduous forest showed markedly higher seasonal variations than evergreen species. Despite these temporal constraints, the fire-induced changes in NDVI were clearly more persistent than changes in α and LST (see Figs 6–8). Except for some winter observations over deciduous forest, the NDVI appears to be a good discriminator between control and focal pixels. In contrast, seasonality dominates the temporal profiles of α and LST variables.

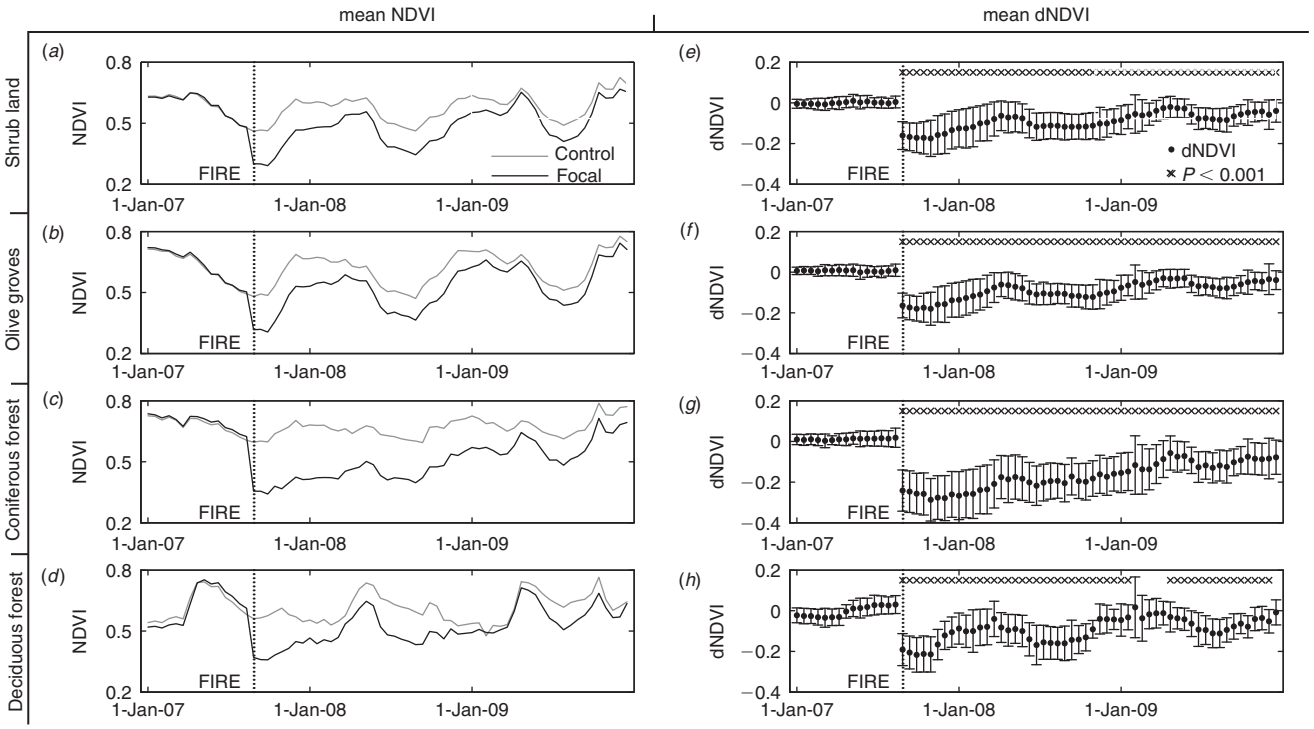

Fig. 5. Two-year post-fire temporal evolution of mean NDVI (Normalised Difference Vegetation Index) of control and focal pixels for shrub land (*a*), olive groves (*b*), coniferous forest (*c*), and deciduous forest (*d*); and 2-year post-fire temporal evolution of mean differenced NDVI (dNDVI) for shrub land (*e*), olive groves (*f*), coniferous forest (*g*), and deciduous forest (*h*). The crosses in (*e–h*) indicate that the mean significantly differs from zero ($P < 0.001$). In (*g–h*), standard deviations are plotted with vertical bars.

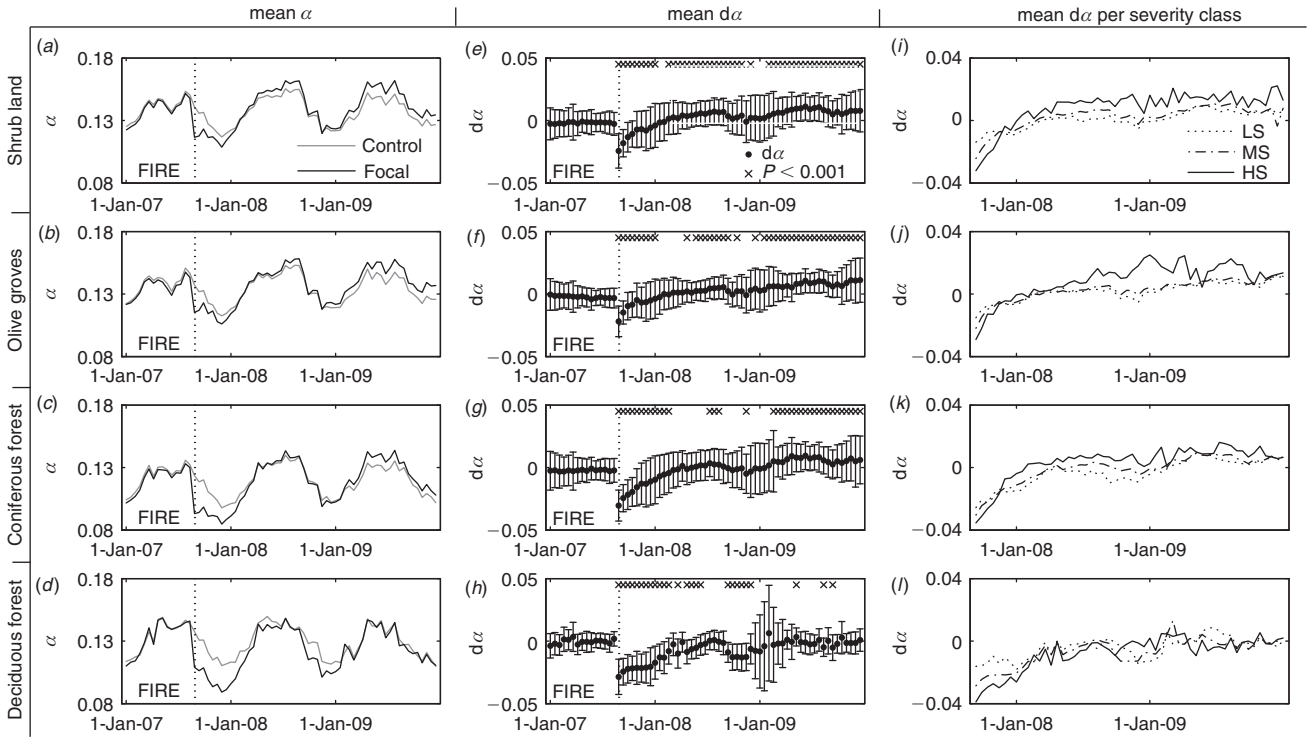

Fig. 6. Two-year post-fire temporal evolution of mean surface albedo α of control and focal pixels for shrub land (*a*), olive groves (*b*), coniferous forest (*c*), and deciduous forest (*d*); 2-year post-fire temporal evolution of mean dα for shrub land (*e*), olive groves (*f*), coniferous forest (*g*), and deciduous forest (*h*); 2-year post-fire temporal evolution of mean differenced α (dα) per fire–burn severity classes for shrub land (*i*), olive groves (*j*), coniferous forest (*k*), and deciduous forest (*l*). The crosses in (*e–h*) indicate that the mean significantly differs from zero ($P < 0.001$). In (*g–h*), standard deviations are plotted with vertical bars. In (*i–l*), LS, MS and HS stand for low, moderate and high severity.

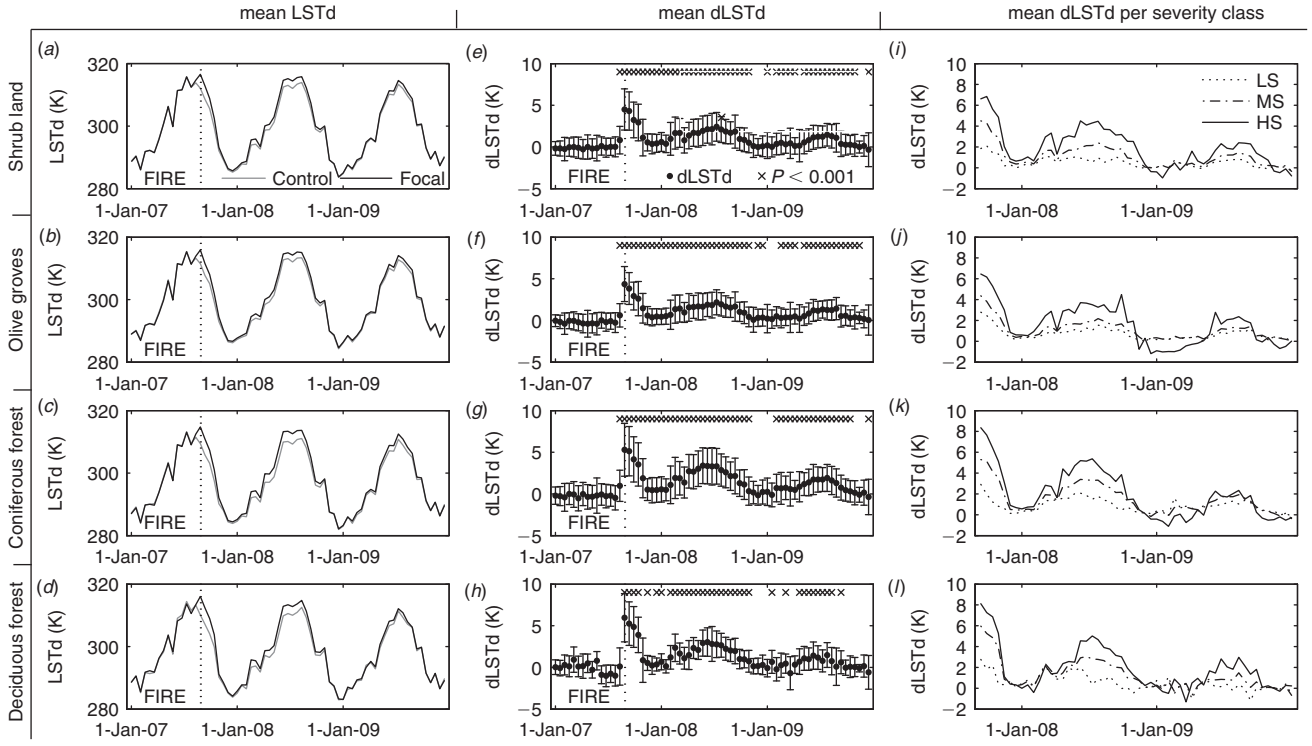

Fig. 7. Two-year post-fire temporal evolution of mean daytime land surface temperature (LSTd) of control and focal pixels for shrub land (*a*), olive groves (*b*), coniferous forest (*c*), and deciduous forest (*d*); 2-year post-fire temporal evolution of mean differenced LSTd (dLSTd) for shrub land (*e*), olive groves (*f*), coniferous forest (*g*), and deciduous forest (*h*); 2-year post-fire temporal evolution of mean dLSTd per fire–burn severity classes for shrub land (*i*), olive groves (*j*), coniferous forest (*k*), and deciduous forest (*l*). The crosses in (*e–h*) indicate that the mean significantly differs from zero ($P < 0.001$). In (*g–h*), standard deviations are plotted with vertical bars. In (*i–l*), LS, MS and HS stand for low, moderate and high severity.

The usefulness of these variables to discriminate between fire-affected areas, thus heavily depends on assessment timing.

Post-fire α changes

The effects of fire on α are multiple. First, an immediate post-fire decrease in α was observed. This decrease was up to 0.039 (0.012) for the HS class in deciduous forest. This outcome is in line with previously published findings that report α drops in the range of 0.01–0.05 (Beringer *et al.* 2003; Jin and Roy 2005; Amiro *et al.* 2006*a*; Lyons *et al.* 2008). Two of these studies were also based on MODIS imagery (Jin and Roy 2005; Lyons *et al.* 2008). Lyons *et al.* (2008) observed a slight decrease of 0.012 (0.005), whereas the average α drop of 0.024 reported by Jin and Roy (2005) more closely approximates our values. The main reason for the immediate post-fire α decrease is the large-scale replacement of living vegetation with black carbon on the surface. Char materials strongly absorb the incoming sunlight and as such, they cause a significant reduction of the reflection-to-incoming sunlight ratio. However, this effect had a relatively short duration, as during the first post-fire winter period, which is a period of heavy rainfall in the Mediterranean, most of the char materials are removed by fluvial and aeolian forces (Pereira *et al.* 1999). In Fig. 6, one can see that the control pixel α values reveal a typical seasonality, which is closely connected with moisture conditions. The α values are clearly lower during wet winter periods than during dry summer periods. However, as shown in Fig. 6, α values of undisturbed plots do not significantly differ from those of burned plots during winter. This suggests, in contrast to findings of Tsuyuzaki *et al.* (2009), that the seasonal variations in surface moisture and the removal of black carbon more strongly drive the α recovery than the early regeneration of vegetation. It is, however, also recognised that leaves and branches of regenerating species have a higher α than mature species (Betts and Ball 1997; Amiro *et al.* 2006*b*). The combination of char removal and regenerating species causes an α increase during the post-fire summer periods. This increase was even more evident for the second post-fire summer than for the first. This can be explained by the fact that after the first winter period, most surface char coating has been removed and early vegetation regeneration has started, but after the second winter period, even more of this char material is ablated and vegetation continues regenerating. This implies the exposure of highly reflective soil and rock combined with regenerating species, which results in an α increase (Lyons *et al.* 2008). These changes in post-fire summer α depend on fire–burn severity. The magnitude of summer α change is proportionally related to the degree of severity (see Fig. 5). In a long-term study (30 years post-fire), Amiro *et al.* (2006*a*) ascertained that the α increase progressively weakens as regenerating vegetation matures. Thus, where the immediate fire effect results in an increased absorption of radiative energy, the long-term effect generally is an increased albedo (Amiro *et al.* 2006*a*; Randerson *et al.* 2006). The quantification of these effects, together with an accurate estimation of the amount of greenhouse gases emitted

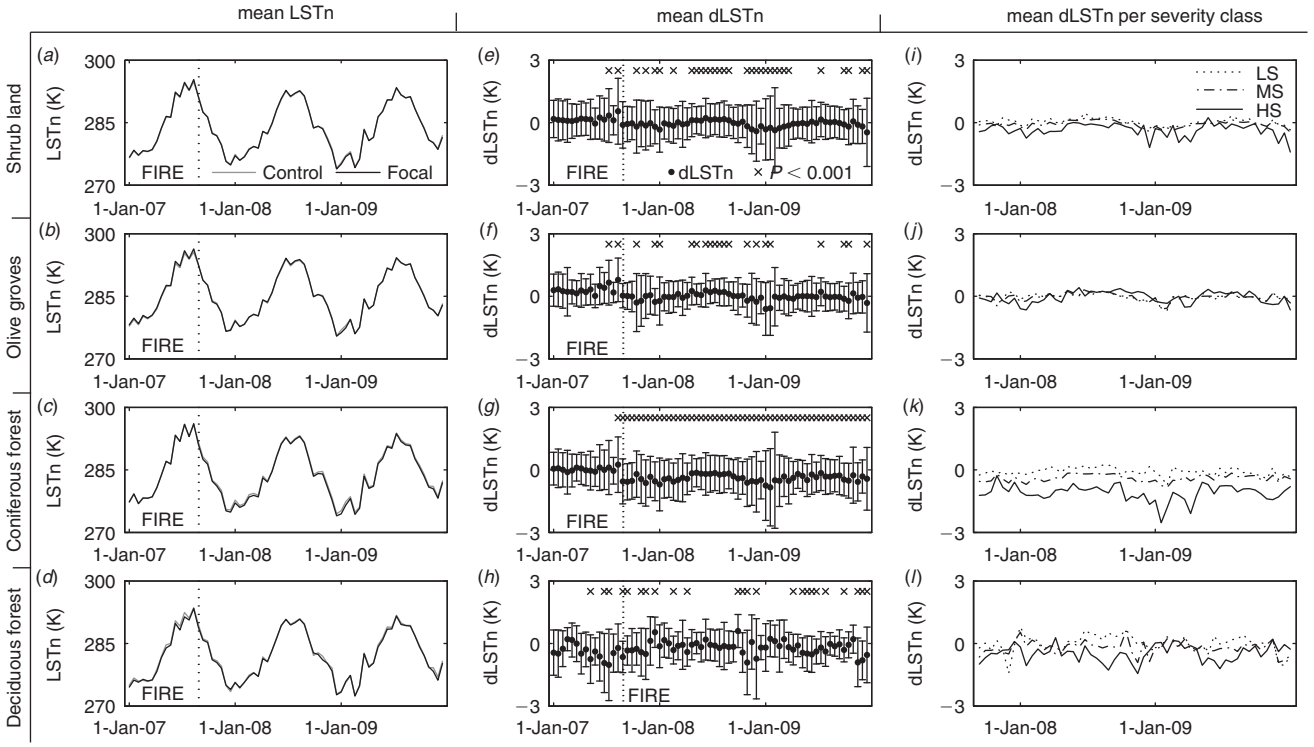

Fig. 8. Two-year post-fire temporal evolution of mean night-time land surface temperature (LSTn) of control and focal pixels for shrub land (*a*), olive groves (*b*), coniferous forest (*c*), and deciduous forest (*d*); 2-year post-fire temporal evolution of mean dLSTn for shrub land (*e*), olive groves (*f*), coniferous forest (*g*), and deciduous forest (*h*); 2-year post-fire temporal evolution of mean differenced LSTn (dLSTn) per fire–burn severity classes for shrub land (*i*), olive groves (*j*), coniferous forest (*k*), and deciduous forest (*l*). The crosses in (*e*–*h*) indicate that the mean significantly differs from zero ($P < 0.001$). In (*g*–*h*), standard deviations are plotted with vertical bars. In (*i*)–(*l*), LS, MS and HS stand for low, moderate and high severity.

by the fire and the subsequent post-fire carbon sequestration of regenerating vegetation, are necessary for holistic comprehension of the effect of wildfires on regional and global climate. In this context, Randerson *et al.* (2006) comprehensively demonstrated that, although the first post-fire year resulted in net warming, the long-term balance was negative. As such, they concluded that increasing fire activity in the boreal region would not necessarily lead to net climate warming. However, these findings were restricted to the boreal eco-region and a similar net balance has not yet been formulated for more quickly recovering ecosystems, such as in fire-prone (sub)tropical and Mediterranean regions.

Post-fire LST changes

Besides assessing fire-induced changes in LST with respect to lag and seasonal timing, MODIS imagery also permits a study of diurnal differences. Immediately post-fire, LSTd increases. The magnitude of this increase depends on land cover and fire–burn severity class. For the HS class of coniferous forest, the focal pixels mean exceeded the control pixels mean by 8.4 (3.0) K. This is very similar to the 2–8 K immediate post-fire temperature daytime temperature increases reported by other studies (Lopez García and Caselles 1991; Cahoon *et al.* 1994; Eva and Lambin 1998; Amiro *et al.* 1999; Bremer and Ham 1999; Lambin *et al.* 2003; Wendt *et al.* 2007; Montes-Helu *et al.* 2009). This effect has, however, only a very short duration, as by the onset of the wet winter, LSTd differences are minor. These findings corroborate an analogous study that assessed the influence of deforestation on LSTd (Manoharan *et al.* 2009). The latter authors reported that LSTd is 4 to 8 K higher during the dry season for deforested regions compared with nearby forests. However, during the wet season, LSTd of deforested and forested plots reach similar values. One can infer the same trend from Fig. 6. During the 1-year and subsequent post-fire summer seasons, mean LSTd increases strongly decline. This attenuation can be attributed to vegetation regeneration processes (see Fig. 4) and char removal. The summer LSTd increase is the driving force of the synchronous increase in sensible and ground heat fluxes (Wendt *et al.* 2007). Little research has been conducted so far to assess the post-fire changes in LSTn. The range of changes in LSTn is relatively small. This makes it difficult to infer post-fire trends for this variable. The fire-induced changes in LSTn are only persistent over coniferous forest. For this cover type, a clear relation between fire–burn severity and dLSTn also exists. During the 1-year post-fire winter, for example, LSTn drops −1.4 (1.0) K for the HS class over coniferous forest. It is important to mention that the MVC criterion favours the detection of post-fire LST increases, whereas it diminishes the observation of cold extremes. This potentially results in a slight underestimation of the post-fire LSTn decrease. In general, fire, thus, creates a more extreme environment with warmer days and colder nights. Another striking result lies in the fact that both dLSTn and dLSTd

observations of the last prefire composite of the evergreen cover types are significantly higher than zero. This potentially opens opportunities to use remotely sensed LST data as a real-time fire risk indicator (Manzo-Delgado *et al.* 2009).

Relation between fire-induced changes in α, LST and fire–burn severity

Fire-induced changes in α and LST show a marked seasonality. This results in significant changes immediately post-fire and in summer periods and insignificant differences during winter periods. Changes in NDVI, in contrast, are clearly more persistent. For α and LST, the magnitude of fire-induced changes is smaller than seasonal amplitude, whereas for VIs, the post-fire drop dominates the temporal profiles. This raises questions about the proposal of Lyons *et al.* (2008) to use pre- and post-fire differenced satellite-derived albedo data as an indicator of fire–burn severity. Fire–burn severity assessment timing is already a serious issue when working with VIs (Key 2006; Verbyla *et al.* 2008; Veraverbeke *et al.* 2010*a*). Introducing biophysical parameters with high seasonal amplitude would only hamper this more, especially because fire–burn severity is traditionally estimated based on Landsat imagery (French *et al.* 2008), which is frequently affected by cloudy observations (Ju and Roy 2008). Only the first post-fire observation of these variables shows some potential to be used a fire severity indicator. Additionally, changes in LST are not only dependent on a plot fire–burn severity but also on the meteorological conditions of the acquisition period. This feature limits the comparability of LST changes of different fires across space and time. For the times when changes in α and LSTd are significant, the magnitude of these changes indeed has a very close relation with a plot's fire–burn severity, as estimated by its NDVI change (see Figs 6–8). This emphasises the importance of vegetation as an important regulator of surface energy fluxes (Xiao and Weng 2007; Amiri *et al.* 2009; Manoharan *et al.* 2009; Tsuyuzaki *et al.* 2009). Fire thus creates a more arid environment with enhanced diurnal and seasonal temperature fluctuations. Vegetation regeneration, however, progressively tempers this effect and facilitates long-term ecosystem recovery (Amiro *et al.* 2006*a*; Tsuyuzaki *et al.* 2009). Although the immediate post-fire changes in α and LSTd observed in the present study are consistent with results obtained in other ecosystems (among others Jin and Roy 2005; Lyons *et al.* 2008; Lopez García and Caselles 1991; Cahoon *et al.* 1994; Eva and Lambin 1998; Amiro *et al.* 1999; Bremer and Ham 1999; Lambin *et al.* 2003; Wendt *et al.* 2007; Montes-Helu *et al.* 2009), our analysis also incorporated seasonal changes. To date, few studies have assessed the interaction between fire-provoked changes and seasonality. It is obviously recognised that this seasonality depends on the regional climate. In regions experiencing a prominent period of snow cover, this feature will heavily influence seasonal cycles of energy fluxes (Betts and Ball 1997).

Conclusions

In this study, the pixel-based control plot selection procedure allowed a multitemporal assessment of the effects of the 2007 Peloponnese (Greece) wildfires on local climate during a 2-year post-fire period based on MODIS satellite imagery. Post-fire changes in vegetation, α and LST were dependent on land-cover type and fire–burn severity. Post-fire NDVI time series were dominated by their post-fire NDVI drop, whereas changes in α and LST were highly dependent on seasonality. Therefore, VIs are more effective to detect burns and to distinguish severity levels. Surface α sharply decreased immediately after the fire event; however, during the subsequent summer period, α increased, whereas during winter, α changes were minimal. LSTd was higher after the fire. This increase was especially obvious during summer periods. The temperature increase became smaller as time elapsed as a consequence of regenerating vegetation. Changes in LSTn were very small and almost not significant, except over coniferous forest, where LSTn slightly decreased. The magnitude of these changes is proportionally related to a plot's fire–burn severity, as assessed by the post-fire NDVI drop. This study provides insights on the multitemporal changes in energy fluxes in a fire-altered environment, which have important ecological implications.

Acknowledgements

The study was initially financed by the Ghent University special research funds (BOF, Bijzonder Onderzoeksfonds). Part of the work was carried out at the Jet Propulsion Laboratory (JPL), California Institute of Technology, under a contract with the National Aeronautics and Space Administration. We are indebted to the reviewers and the editor for their constructive remarks, which resulted in an improved manuscript. The JPL author's copyright for this publication is held by the California Institute of Technology.

References

Amiri R, Weng Q, Alimohammadi A, Kazem Alavipanah S (2009) Spatial–temporal dynamics of land surface temperature in relation to fractional cover and land use/cover in the Tabriz urban area, Iran. *Remote Sensing of Environment* **113**, 2606–2617. doi:10.1016/J.RSE.2009.07.021

Amiro B, MacPherson J, Desjardins R (1999) BOREAS flight measurements of forest-fire effects on carbon dioxide and energy fluxes. *Agricultural and Forest Meteorology* **96**, 199–208. doi:10.1016/S0168-1923(99)00050-7

Amiro B, Barr A, Black T, Iwashita H, Kljun N, McCaughey J, Morgenstern K, Muruyama S, Nesic Z, Orchansky A, Saigusa N (2006*a*). Carbon, energy and water fluxes at mature and disturbed forest sites, Saskatchewan, Canada. *Agricultural and Forest Meteorology* **136**, 237–251. doi:10.1016/J.AGRFORMET.2004.11.012

Amiro B, Orchansky A, Barr A, Black T, Chambers S, Chapin F, Goulden M, Litvak M, Liu H, McCaughey J, McMillan A, Randerson J (2006*b*). The effect of post-fire stand age on the boreal forest energy balance. *Agricultural and Forest Meteorology* **140**, 41–50. doi:10.1016/J.AGRFORMET.2006.02.014

Barbosa P, Gregoire J, Pereira J (1999) An algorithm for extracting burned areas from time series of AVHRR GAC data applied at a continental scale. *Remote Sensing of Environment* **69**, 253–263. doi:10.1016/S0034-4257(99)00026-7

Beringer J, Hutley L, Tapper N, Coutts A, Kerley A, O'Grady A (2003) Fire impacts on surface heat, moisture and carbon fluxes from a tropical savanna in northern Australia. *International Journal of Wildland Fire* **12**, 333–340. doi:10.1071/WF03023

Betts A, Ball J (1997) Albedo over the boreal forest. *Journal of Geophysical Research* **102**, 28 901–28 609. doi:10.1029/96JD03876

Boer M, MacFarlane C, Norris J, Sadler R, Wallace J, Grierson P (2008) Mapping burned areas and burn severity patterns in SW Australian

eucalypt forest using remotely sensed changes in leaf area index. *Remote Sensing of Environment* **112**, 4358–4369. doi:10.1016/J.RSE.2008.08.005

Bowen I (1926) The ratio of heat losses by conduction and by evaporation from any water surface. *Physical Review* **27**, 779–787. doi:10.1103/PHYSREV.27.779

Bremer D, Ham J (1999) Effect of spring burning on the surface energy balance in a tallgrass prairie. *Agricultural and Forest Meteorology* **97**, 43–54. doi:10.1016/S0168-1923(99)00034-9

Cahoon D, Stocks B, Levine J, Cofer W, Pierson J (1994) Satellite analysis of the severe 1987 forest fires in northern China and south-eastern Siberia. *Journal of Geophysical Research* **99**, 18 627–18 638. doi:10.1029/94JD01024

Capitanio R, Carcaillet C (2008) Post-fire Mediterranean vegetation dynamics and diversity: a discussion of succession models. *Forest Ecology and Management* **255**, 431–439. doi:10.1016/J.FORECO.2007.09.010

Chafer C, Noonan M, Macnaught E (2004) The post-fire measurement of fire severity and intensity in the Christmas 2001 Sydney wildfires. *International Journal of Wildland Fire* **13**, 227–240. doi:10.1071/WF03041

Chuvieco E, Englefield P, Trishchenko A, Luo Y (2008) Generation of long time series of burn area maps of the boreal forest from NOAA–AVHRR composite data. *Remote Sensing of Environment* **112**, 2381–2396. doi:10.1016/J.RSE.2007.11.007

Díaz-Delgado R, Pons X (2001) Spatial patterns of forest fires in Catalonia (NE of Spain) along the period 1975–1995: analysis of vegetation recovery after fire. *Forest Ecology and Management* **147**, 67–74. doi:10.1016/S0378-1127(00)00434-5

Díaz-Delgado R, Lloret F, Pons X (2003) Influence of fire severity on plant regeneration by means of remote sensing. *International Journal of Remote Sensing* **24**, 1751–1763. doi:10.1080/01431160210144732

Dwyer E, Perreira J, Grégoire J, DaCamara C (2000) Characterization of the spatiotemporal patterns of global fire activity using satellite imagery for the period April 1992 to March 1993. *Journal of Biogeography* **27**, 57–69. doi:10.1046/J.1365-2699.2000.00339.X

Epting J, Verbyla D (2005) Landscape-level interactions of prefire vegetation, burn severity, and post-fire vegetation over a 16-year period in interior Alaska. *Canadian Journal of Forest Research* **35**, 1367–1377. doi:10.1139/X05-060

Epting J, Verbyla D, Sorbel B (2005) Evaluation of remotely sensed indices for assessing burn severity in interior Alaska using Landsat TM and ETM+. *Remote Sensing of Environment* **96**, 328–339. doi:10.1016/J.RSE.2005.03.002

Escuin S, Navarro R, Fernandez P (2008) Fire severity assessment by using NBR (Normalized Burn Ratio) and NDVI (Normalized Difference Vegetation Index) derived from LANDSAT TM/ETM images. *International Journal of Remote Sensing* **29**, 1053–1073. doi:10.1080/01431160701281072

European Commission (2005) 'Soil Atlas of Europe.' (Office for Official Publications of the European Communities: Luxembourg)

Eva H, Lambin E (1998) Burnt area mapping in Central Africa using ATSR data. *International Journal of Remote Sensing* **19**, 3473–3497. doi:10.1080/014311698213768

French N, Kasischke E, Hall R, Murphy K, Verbyla D, Hoy E, Allen J (2008) Using Landsat data to assess fire and burn severity in the North American boreal forest region: an overview and summary of results. *International Journal of Wildland Fire* **17**, 443–462. doi:10.1071/WF08007

Hammill K, Bradstock R (2006) Remote sensing of fire severity in the Blue Mountains: influence of vegetation type and inferring fire intensity. *International Journal of Wildland Fire* **15**, 213–226. doi:10.1071/WF05051

Hanes T (1971) Succession after fire in the chaparral of southern California. *Ecological Monographs* **41**, 27–52. doi:10.2307/1942434

Hernández Clemente R, Navarro Cerrillo R, Gitas I (2009) Monitoring post-fire regeneration in Mediterranean ecosystems by employing multitemporal satellite imagery. *International Journal of Wildland Fire* **18**, 648–658. doi:10.1071/WF07076

Higgins M, Higgins R (1996) 'A Geological Companion to Greece and the Aegean.' (Cornell University Press: Ithica, NY)

Holben B (1986) Characteristics of maximum-value composite images from temporal AVHRR data. *International Journal of Remote Sensing* **7**, 1417–1434. doi:10.1080/01431168608948945

Huete A, Didan K, Miura T, Rodriguez E, Gao X, Ferreira L (2002) Overview of the radiometric and biophysical performance of the MODIS vegetation indices. *Remote Sensing of Environment* **83**, 195–213. doi:10.1016/S0034-4257(02)00096-2

Institute of Geology and Mineral Exploration (1983) 'Geological Map of Greece 1 : 500 000.' (Ordnance Survey: Southampton, UK)

Isaev A, Korovin G, Bartalev S, Ershov D, Janetos A, Kasischke E, Shugart H, French N, Orlick B, Murphy T (2002) Using remote sensing to assess Russian forest fire carbon emissions. *Climatic Change* **55**, 235–249. doi:10.1023/A:1020221123884

Jin Y, Roy D (2005) Fire-induced albedo-change and its radiative forcing at the surface in northern Australia. *Geophysical Research Letters* **32**, L13401. doi:10.1029/2005GL022822

Jonsson P, Eklundh L (2004) TIMESAT – a program for analyzing time-series of satellite sensor data. *Computers & Geosciences* **30**, 833–845. doi:10.1016/J.CAGEO.2004.05.006

Ju J, Roy D (2008) The availability of cloud-free Landsat ETM+ data over the conterminous United States and globally. *Remote Sensing of Environment* **112**, 1196–1211. doi:10.1016/J.RSE.2007.08.011

Justice C, Townshend J, Vermote E, Masuoka E, Wolfe R, Saleous N, Roy D, Morisette J (2002) An overview of MODIS land data processing and products status. *Remote Sensing of Environment* **83**, 3–15. doi:10.1016/S0034-4257(02)00084-6

Keeley J (2009) Fire intensity, fire severity and burn severity: a brief review and suggested usage. *International Journal of Wildland Fire* **18**, 116–126. doi:10.1071/WF07049

Key C (2006) Ecological and sampling constraints on defining landscape fire severity. *Fire Ecology* **2**, 34–59. doi:10.4996/FIREECOLOGY.0202034

Key C, Benson N (2005) Landscape assessment: ground measure of severity; the Composite Burn Index, and remote sensing of severity, the Normalized Burn Index. In 'FIREMON: Fire Effects Monitoring and Inventory System'. (Eds D Lutes, R Keane, J Caratti, C Key, N Benson, S Sutherland, L Grangi) USDA Forest Service, Rocky Mountains Research Station, General Technical Report RMRS-GTR-164-CD LA, pp. 1–51. (Fort Collins, CO)

Lambin E, Goyvaerts K, Petit C (2003) Remotely sensed indicators of burning efficiency of savannah and forest fires. *International Journal of Remote Sensing* **24**, 3105–3118. doi:10.1080/0143116021000021224

Lentile L, Smith F, Shepperd W (2005) Patch structure, fire-scar formation, and tree regeneration in a large mixed-severity fire in the South Dakota Black Hills, USA. *Canadian Journal of Forest Research* **35**, 2875–2885. doi:10.1139/X05-205

Lentile L, Holden Z, Smith A, Falkowski M, Hudak A, Morgan P, Lewis S, Gessler P, Benson N (2006) Remote sensing techniques to assess active fire characteristics and post-fire effects. *International Journal of Wildland Fire* **15**, 319–345. doi:10.1071/WF05097

Lhermitte S, Verbesselt J, Verstraeten WW, Coppin P (2010) A pixel-based regeneration index using time series similarity and spatial context. *Photogrammetric Engineering and Remote Sensing* **76**, 673–682.

Lhermitte S, Verbesselt J, Verstraeten WW, Veraverbeke S, Coppin P (2011) Assessing intra-annual vegetation regrowth using the pixel-based regeneration index. *ISPRS Journal of Photogrammetry and Remote Sensing* **66**, 17–27. doi:10.1016/J.ISPRSJPRS.2010.08.004

Lopez García M, Caselles V (1991) Mapping burns and natural reforestation using Thematic Mapper data. *Geocarto International* **6**, 31–37. doi:10.1080/10106049109354290

Lyons E, Jin Y, Randerson J (2008) Changes in surface albedo after fire in boreal forest ecosystems of interior Alaska assessed using MODIS satellite observations. *Journal of Geophysical Research* **113**, G02012. doi:10.1029/2007JG000606

Manoharan V, Welch R, Lawton R (2009) Impact of deforestation on regional surface temperature and moisture in the Maya lowlands of Guatemala. *Geophysical Research Letters* **36**, L21701. doi:10.1029/2009GL040818

Manzo-Delgado L, Sanchez-Colon S, Alvarez R (2009) Assessment of seasonal forest fire risk using NOAA-AVHRR: a case study in central Mexico. *International Journal of Remote Sensing* **30**, 4991–5013. doi:10.1080/01431160902852796

Miller J, Thode A (2007) Quantifying burn severity in a heterogeneous landscape with a relative version of the delta Normalized Burn Ratio (dNBR). *Remote Sensing of Environment* **109**, 66–80. doi:10.1016/J.RSE.2006.12.006

Montes-Helu M, Kolb T, Dore S, Sullivan B, Hart S, Koch G, Hungate B (2009) Persistent effects of fire-induced vegetation change on energy partioning in ponderosa pine forests. *Agricultural and Forest Meteorology* **149**, 491–500. doi:10.1016/J.AGRFORMET.2008.09.011

Moretti M, Conedera M, Duelli P, Edwards P (2002) The effect of wildfire on ground-active spiders in deciduous forests on the Swiss southern slope of the Alps. *Journal of Applied Ecology* **39**, 321–336. doi:10.1046/J.1365-2664.2002.00701.X

Pausas J (2004) Changes in fire and climate in the eastern Iberian peninsula (Mediterranean Basin). *Climatic Change* **63**, 337–350. doi:10.1023/B:CLIM.0000018508.94901.9C

Pereira J, Sa A, Sousa A, Silva J, Santos T, Carreiras J (1999). Spectral characterization and discrimination of burnt areas. In 'Remote Sensing of Large Wildfires in the European Mediterranean Basin'. (Ed. E Chuvieco) pp. 123–138. (Springer-Verlag: Berlin)

Randerson J, Liu H, Flanner M, Chamber S, Jin Y, Hess P, Pfister G, Mack M, Treseder K, Welp L, Chapin F, Harden J, Goulden M, Lyons E, Neff J, Schuur E, Zender C (2006) The impact of boreal forest fire on climate warming. *Science* **314**, 1130–1132. doi:10.1126/SCIENCE.1132075

Riaño D, Moreno-Ruiz J, Isidoros D, Ustin S (2007) Global spatial patterns and temporal trends of burned area between 1981 and 2000 using NOAA-NASA Pathfinder. *Global Change Biology* **13**, 40–50. doi:10.1111/J.1365-2486.2006.01268.X

Savitzky A, Golay M (1964) Smoothing and differentiation of data by simplified least squares procedures. *Analytical Chemistry* **36**, 1627–1639. doi:10.1021/AC60214A047

Schaaf C, Gao F, Strahler A, Lucht W, Li X, Tsang T, Strugnell N, Zhang X, Jin Y, Muller J, Lewis P, Barnsley M, Hobson P, Disney M, Robert G, Dunderdale M, Doll C, d'Entremont R, Hu B, Liang S, Privette J, Roy D (2002) First operational BRDF, albedo nadir reflectance products from MODIS. *Remote Sensing of Environment* **83**, 135–148. doi:10.1016/S0034-4257(02)00091-3

Stroppiana D, Pinnock S, Pereira J, Gregoire J (2002) Radiometric analysis of SPOT-VEGETATION images for burnt area detection in northern Australia. *Remote Sensing of Environment* **82**, 21–37. doi:10.1016/S0034-4257(02)00021-4

Trabaud L (1981) Man and fire: impacts on Mediterranean vegetation. In 'Mediterranean-type Shrublands'. (Eds F di Castri, D Goodall, R Specht) pp. 523–537. (Elsevier: Amsterdam)

Tsuyuzaki S, Kushida K, Kodama Y (2009) Recovery of surface albedo and plant cover after wildfire in a *Picea mariana* forest in interior Alaska. *Climatic Change* **93**, 517–525. doi:10.1007/S10584-008-9505-Y

van Leeuwen W (2008) Monitoring the effects of forest restoration treatments on post-fire vegetation recovery with MODIS multitemporal data. *Sensors* **8**, 2017–2042. doi:10.3390/S8032017

van Leeuwen W, Casady M, Neary D, Bautista S, Alloza J, Carmel Y, Wittenberg L, Malkinson D, Orr B (2010) Monitoring post-wildfire vegetation response with remotely sensed time-series data in Spain, USA and Israel. *International Journal of Wildland Fire* **19**, 75–93. doi:10.1071/WF08078

Veraverbeke S, Lhermitte S, Verstraeten WW, Goossens R (2010*a*). The temporal dimension of differenced Normalized Burn Ratio (dNBR) fire/burn severity studies: the case of the large 2007 Peloponnese wildfires in Greece. *Remote Sensing of Environment* **114**, 2548–2563. doi:10.1016/J.RSE.2010.05.029

Veraverbeke S, Verstraeten WW, Lhermitte S, Goossens R (2010*b*). Evaluating Landsat Thematic Mapper spectral indices for estimating burn severity of the 2007 Peloponnese wildfires in Greece. *International Journal of Wildland Fire* **19**, 558–569. doi:10.1071/WF09069

Veraverbeke S, Lhermitte S, Verstraeten WW, Goossens R (2010*c*). Illumination effects on the differenced Normalized Burn Ratio's optimality for assessing fire severity. *International Journal of Applied Earth Observation and Geoinformation* **12**, 60–70. doi:10.1016/J.JAG.2009.10.004

Veraverbeke S, Lhermitte S, Verstraeten WW, Goossens R (2011) A time-integrated MODIS burn severity assessment using the multi-temporal differenced Normalized Burn Ratio ($dNBR_{MT}$). *International Journal of Applied Earth Observation and Geoinformation* **13**, 52–58. doi:10.1016/J.JAG.2010.06.006

Verbyla D, Kasischke E, Hoy E (2008) Seasonal and topographic effects on estimating fire severity from Landsat TM/ETM+ data. *International Journal of Wildland Fire* **17**, 527–534. doi:10.1071/WF08038

Viedma O, Melia J, Segarra D, Garcia-Haro J (1997) Modeling rates of ecosystem recovery after fires by using Landsat TM data. *Remote Sensing of Environment* **61**, 383–398. doi:10.1016/S0034-4257(97)00048-5

Wan Z (2008) New refinements and validation of the MODIS land-surface temperature/emissivity products. *Remote Sensing of Environment* **112**, 59–74. doi:10.1016/J.RSE.2006.06.026

Wendt C, Beringer J, Tapper N, Hutley L (2007) Local boundary-layer development over burnt and unburnt tropical savanna: an observational study. *Boundary-Layer Meteorology* **124**, 291–304. doi:10.1007/S10546-006-9148-3

White J, Ryan K, Key C, Running S (1996) Remote sensing of forest fire severity and vegetation recovery. *International Journal of Wildland Fire* **6**, 125–136. doi:10.1071/WF9960125

Xiao H, Weng Q (2007) The impact of land use and land cover changes on land surface temperature in a karst area of China. *Journal of Environmental Management* **85**, 245–257. doi:10.1016/J.JENVMAN.2006.07.016